ELSEVIER

Chemical Engineering Journal 135S (2008) S229–S236

Chemical Engineering Journal

www.elsevier.com/locate/cej

Multiphase flow regimes for hydrogenation in a catalyst-trap microreactor

S. McGovern [a], G. Harish [a], C.S. Pai [b], W. Mansfield [b], J.A. Taylor [b], S. Pau [c], R.S. Besser [a,*]

[a] *Chemical, Biomedical, & Materials Engineering Department, Stevens Institute of Technology, Castle Point on Hudson, Hoboken, NJ 07030, United States*
[b] *New Jersey Nanotechnology Consortium (NJNC) at Lucent-Bell Labs, 600 Mountain Avenue, Murray Hill, NJ 07974, United States*
[c] *University of Arizona, College of Optical Sciences, 1630 East University Blvd., Tuscon, AZ 85721, United States*

Abstract

Multiphase reactions, namely gas–liquid reactions involving solid catalyst, play a critical role in many industries. In particular, hydrogenation reactions are carried out on a large scale in the pharmaceutical industry. Nearly 20% all reaction steps in a typical fine chemical synthesis are catalytic hydrogenation. The use of microreactor geometry would greatly benefit chemical process miniaturization in the pharmaceutical and other industries.

A silicon microreactor has been developed to investigate multiphase mass transfer in the context of gas–liquid–solid catalytic reactions. The reactor employs a three-channel "catalyst-trap" design, whereby solid catalyst is suspended in the liquid channel by an arrangement of posts. Such a device has advantages in that commercial catalysts are supported, and that pressure drop across the bed can be reduced by engineering the packing density. In this paper, a model incorporating the transport and kinetic effects is developed to design this kind of reactor. We have chosen the liquid-phase hydrogenation of *o*-nitroanisole to *o*-anisidine to serve as a prototype reaction. The reaction is carried out across a range of gas and liquid flow rates that encompass three distinct flow regimes, termed gas-dominated, liquid-dominated, and transitional.

Variations of the reactor design are used to study the flow regimes in detail. A two-phase "flow map" is generated for each reactor type. Kinetic experiments seek to assign a reaction conversion to each point in this two-phase "flow map," in order to subsequently reconcile differences in performance with the characteristics of the respective flow regime. We observe the highest reaction conversion in the transitional flow regime, where competition between the two phases results in the generation of a large amount of gas–liquid interfacial area. The experimental conversion is greater than that predicted by the initial plug-flow model, an effect attributable to the mass transfer enhancement induced by transitional flow. Flow maps for each reactor variation show that liquid channel dimensions and trap density can be manipulated to maximize the region of transitional flow. In addition, we explore operation at elevated pressures to enhance hydrogen solubility. This reactor architecture may be useful for catalyst evaluation through rapid screening, or in large numbers as an alternative to macroscale production reactors.

Keywords: Microreactor; Silicon; Packed Bed; Hydrogenation; Multiphase; Gas-Liquid Mass Transfer; Interfacial Area; Mass Transfer Coefficient; Flow Regimes; Transitional Flow; Refreshment Period; Surface Renewal; Pharmaceuticals; Fine Chemicals

1. Introduction

Miniaturization of chemical processes is motivated by the quest for clean and efficient on-site, on-demand, and on-time distributed production of chemicals. To this end, the term "microreactor" is broadly used to describe devices with critical geometry ranging from tens of microns to approximately 1 mm in size. Microreactor technology possesses significant advantages over conventional macroscale reactors. Because of their small size, microreactors have inherently large surface-to-volume ratios, allowing for superior mass and heat transport. Surface-to-volume ratios of 20,000 m^2/m^3 or more are not uncommon, compared to 1000 m^2/m^3 for a conventional reactor. Laminar flow is typically impressed by microgeometry, but because the overall heat transfer coefficient is inversely proportional to channel diameter, values for liquids are on the order of 10,000 $W/(m^2\,K)$, roughly one order of magnitude higher than in conventional heat exchangers [1–8].

In the case of catalytic reactions, where competition exists between the rate of diffusion to the catalyst sites and the rate of reaction, microreactors are able to virtually eliminate mass transport resistance, making them an extremely useful tool for isolating reaction kinetics. Excellent heat transfer properties ensure a uniform temperature throughout the reactor and prevent the formation of hotspots in the case of an exothermic reaction. In a stirred-tank reactor, for example, hotspots can lead to undesired changes in local concentration or pH. Low residence time and ease of heat removal also make microreactors more suitable for flammable service, where the potential for explosion or fire from runaway reactions is greatly reduced [9,10].

* Corresponding author. Tel.: +1 201 216 5257.
E-mail address: rbesser@stevens.edu (R.S. Besser).

1385-8947/$ – see front matter © 2007 Elsevier B.V. All rights reserved.
doi:10.1016/j.cej.2007.07.055

Nomenclature

a_h	gas–liquid interfacial area
c_i	liquid-phase concentration of species
H_i	Henry's law constant for species i
k	reaction rate constant
k_L	liquid-phase mass transfer coefficient
K_i	absorption constant for species i
P_i	partial pressure of species i
t	time
u_L	liquid superficial velocity
w_c	weight of catalyst per unit volume of reactor bed
z	length coordinate
ε	reactor void fraction

In this paper, we consider the use of a microreactor for gas–liquid–solid catalytic reactions, where the rate of diffusion of gas into the liquid phase can also limit the observed reaction rate. Thus, we would like to be able to address both intra- and inter-particle diffusion. The former can be accomplished with reasonable certainty simply by using small-sized catalyst particles. In general, catalyst particles with a diameter smaller than 100 μm (1×10^{-4} m) exhibit sufficiently low transport resistance to enable their use with most reactions [11]. The latter is a function of gas–liquid interfacial area and driving force for transport, both of which depend on the gas–liquid flow regime. Similar to the development of macroscale packed or trickle bed reactors, mass transfer in two-phase flow has been studied extensively in microchannel or capillary geometry, and here we wish to extend these principles to reactive systems.

For our purposes, three traditional flow regimes are adequate to describe the two-phase behavior, although other papers present more precise delineations [12–17]. Bubble flow is characterized by liquid as the continuous phase, with bubbles of gas dispersed into a fully wetted channel. As the ratio of gas-to-liquid velocity increases, the Taylor (slug) flow regime emerges, in which alternating segments of gas and liquid occupy the channel. The relative lengths of each segment are constant for a given set of inlet conditions. As gas-to-liquid velocity further increases, annular (for a capillary) or trickle (for a wide reaction channel) flow occurs. In annular or trickle flows, gas is the continuous phase, and the liquid flows as a thin film along the channel walls [12–17]. Analogs of these distinct flow regimes develop within both macro- and microscale devices over varying gas and liquid ratios. Fig. 1 illustrates the three flow regimes, where u_G and u_L are the gas and liquid superficial velocities, respectively.

In the context of a gas–liquid–solid catalytic reaction with reaction occurring in the liquid phase, two characteristics are critical in evaluating the advantages and disadvantages of a particular flow regime. First, we desire good mass transport between gas and liquid, which depends on the driving force for mass transport and the gas–liquid interfacial area created. Second, we desire a high liquid–solid interfacial area to effectively utilize the catalyst for rate of production. The highest liquid–solid interfacial area will be achieved when liquid is the continuous phase.

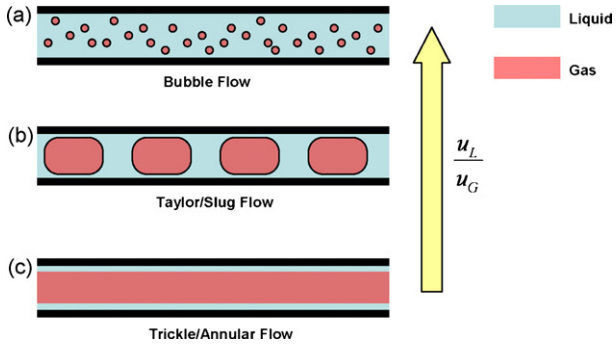

Fig. 1. Illustration of gas/liquid flow regimes.

Taking the example of a capillary, the slug flow regime is typically associated with the best gas–liquid mass transport because of the high shear rates that have been observed to develop between liquid slugs and their intervening fluid [12–17]. The high velocity gradient within the liquid slug provides a chaotic mixing effect, so a constant refreshing of the gas–liquid interface occurs. This provides a high driving force for diffusion of gas across the interface. Despite good mass transport properties, slug flow does not maximize the liquid–solid interfacial area because gas still occupies a significant portion of the channel. Bubble flow, in contrast, exhibits both a high liquid–solid and gas–liquid interfacial area. Because liquid is the continuous phase with only a relatively small fraction of gas present, essentially all of the catalyst is in contact with liquid [18]. Thus, we can generalize that slug flow will possess the best gas–liquid mass transport, owing to both interfacial area and driving force, and that bubble flow, although less turbulent, will have the highest liquid–solid interfacial area. On the basis of these mass transfer arguments, we speculate that the best reactor performance will fall in either the bubble or slug flow regimes. Likewise, we suppose that trickle flow, with the lowest liquid–solid and gas–liquid interfacial areas, will be the least effective for these types of reactions. We proceed to design the device and subsequent experiments with this hypothesis in mind.

2. Reactor modeling, design, and fabrication

The reactor is designed for operation across the spectrum of flow regimes, while making use of the advantages of microchemical systems to relieve various transport resistances. The design is pictured in Fig. 2.

The reactor is used for the liquid-phase hydrogenation of *o*-nitroanisole to *o*-anisidine, with methanol as an inert solvent. The catalyst is 5% Pd by weight on carbon. Hydrogen gas enters along the two outside channels, and is allowed to diffuse into the liquid channel through a slotted wall, shown at the top inset. The reaction occurs in the liquid channel, where an arrangement of posts, or catalyst traps, holds the catalyst particles in place (Fig. 2b, lower inset). Each trap is a trapezoidal arrangement of four posts spanning the depth of the channel. The posts are spaced to "catch" catalyst particles during the catalyst loading process and hold them in place during the reaction processing, so one can imagine the liquid sees the particles stacked single-file

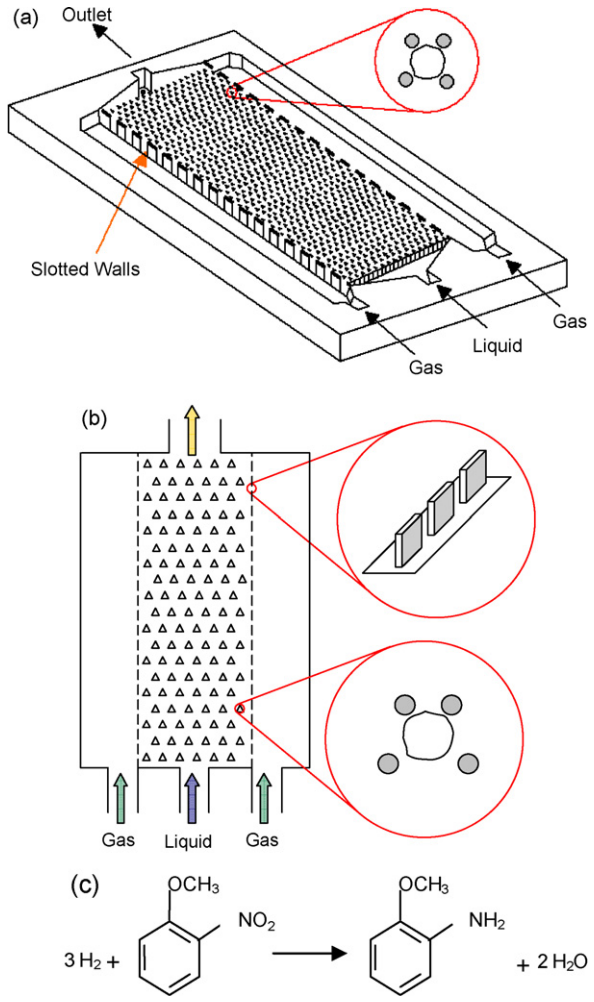

Fig. 2. Proposed reactor design: (a) three-dimensional view; (b) overhead view of channels; (c) reaction.

on top of one another as it travels down the channel. The reaction is therefore a three-step process: (1) hydrogen diffuses through the slots and dissolves in the bulk liquid; (2) the liquid disperses to the catalyst particles and diffuses within the particles to the reaction sites; (3) reaction occurs at the catalyst sites.

To design the reactor, we model the bulk liquid-phase concentration of all species throughout the reactor. The liquid channel is treated as a plug-flow reactor with a continuous source of hydrogen available at any axial position. The slots are sized to allow the gas to overcome liquid surface tension and pass into the liquid channel. Hydrogen concentration in the liquid phase is therefore limited by diffusion across the gas–liquid interface. The rate of change of hydrogen concentration has two contributing terms:

$$\frac{dc_A}{dt} = [\text{rate of diffusion from gas into liquid}] + [\text{rate of reaction}] \quad (1)$$

$$\frac{dc_A}{dz} = \frac{\varepsilon}{u_L}\left[k_L\left(\frac{P_A}{H_A} - c_A\right)a_h - \frac{3w_c k c_A c_B}{(1 + K_A c_A)(1 + K_B c_B)}\right] \quad (2)$$

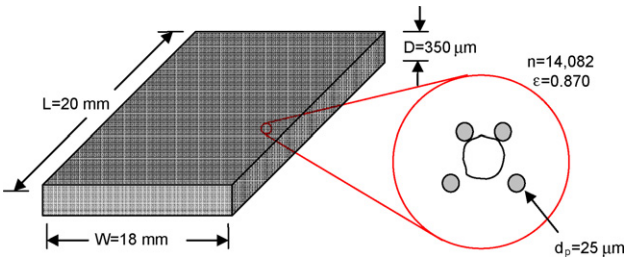

Fig. 3. Design parameters for liquid channel.

For the first term of Eq. (1), the concentration of hydrogen at the gas–liquid interface is calculated from the Henry's law constant, H_A, for hydrogen in solutions of nitroanisole and methanol [19]. The difference between the interfacial and bulk liquid concentrations represents the driving force for diffusion. The parameter a_h is the gas–liquid interfacial area per unit volume, and is estimated from packed tower (stripper/absorber) literature [20]. Uncertainty exists in the application of these macroscale correlations to the microreactor geometry, but in the absence of alternatives we use them for design purposes. The second term is the reaction rate expression [21]. For each remaining species, Eq. (2) contains only the reaction term with the respective stoichiometric coefficient. The four expressions for rate of change of concentration are integrated numerically over the channel length from 0 to z. Fig. 3 shows the final liquid channel dimensions.

The dimensions in Fig. 3 are chosen to give an appreciable conversion across our target range of experimental conditions. The channel contains approximately 14,000 catalyst traps that, when loaded, give a void fraction of 0.870. The posts are 25 μm in diameter and are arranged as a trapezoid to hold a 35–50 μm particle. Traps are spaced 75 μm apart (closest edge-to-edge distance) to allow untrapped catalyst to pass between traps during loading.

The above dimensions constitute the primary reactor design that was used for kinetic experiments. Two variations of this design were also fabricated to study the effect of reactor geometry on the gas–liquid flow regime. The first variation used 150 μm trap spacing. The second used 150 μm trap spacing with a 10 mm liquid channel width. The larger trap spacing was intended to increase void fraction within the channel, thereby decreasing resistance to flow. The narrow liquid channel was intended to observe the effect of decreased resistance to hydrogen diffusion across the channel width. Fig. 4 shows each of the three designs, and Table 1 summarizes the key design parameters of each.

Table 1
Reactor design parameters

	Design parameters			Channel depth (μm)
	Catalyst bed dimensions (mm)	Number of traps	Trap spacing (μm)	
Reactor A	20 × 18	14,082	75	300
Reactor B	20 × 18	6,426	150	300
Reactor C	20 × 10	3,806	150	300

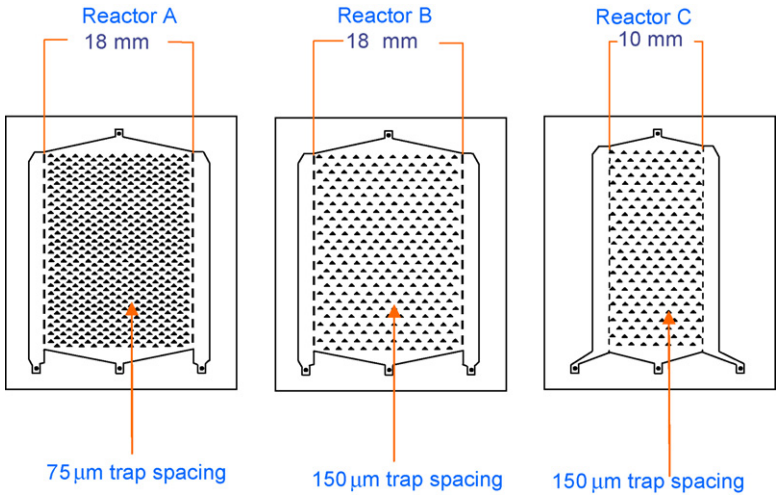

Fig. 4. Variations in reactor design.

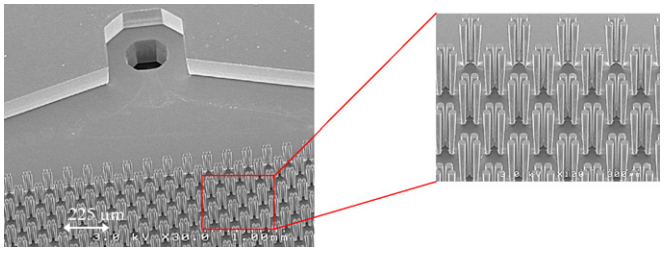

Fig. 5. SEM images of microreactor.

The reactors were fabricated at NJNC-Bell Labs in Murray Hill, NJ using 248 nm and contact lithography and deep reactive ion etching (DRIE). Inlet and outlet ports were etched on the underside of the reactors. After etching, the silicon wafer was diced into individual chips. In our case, we received sixteen chips of dimensions 31 mm × 28 mm (0.031 m × 0.028 m) per 8 in. diameter wafer. The reactors were then sealed by anodically bonding a piece of Pyrex glass over the surface of the chip. Anodic bonding applies voltage at high temperature, typically 1000 V dc and 450–490 °C, to displace ions from the surface of the glass. The depletion of ions makes the glass surface highly reactive, forming a strong bond with the silicon substrate. The intent of the glass-covered reactor is two-fold, first as an aid in catalyst loading, and second for observation of the gas–liquid flow behavior. Fig. 5 shows scanning electron microscope (SEM) images of the completed reactor.

3. Experimental

A schematic of the experimental setup is shown in Fig. 6. For overhead image and video capture, the setup includes a CCD camera above the reactor. The reactor itself is clamped onto a 4.5 in. × 3 in. stainless steel block, through which channels are machined for gas and liquid passage.

We first performed a systematic assessment, or map, of the possible flow regimes as they pertained to our particular devices. To construct the flow maps, we used a range of liquid flow rates in accordance with the model, from 0.06 to 0.50 mL/min, and

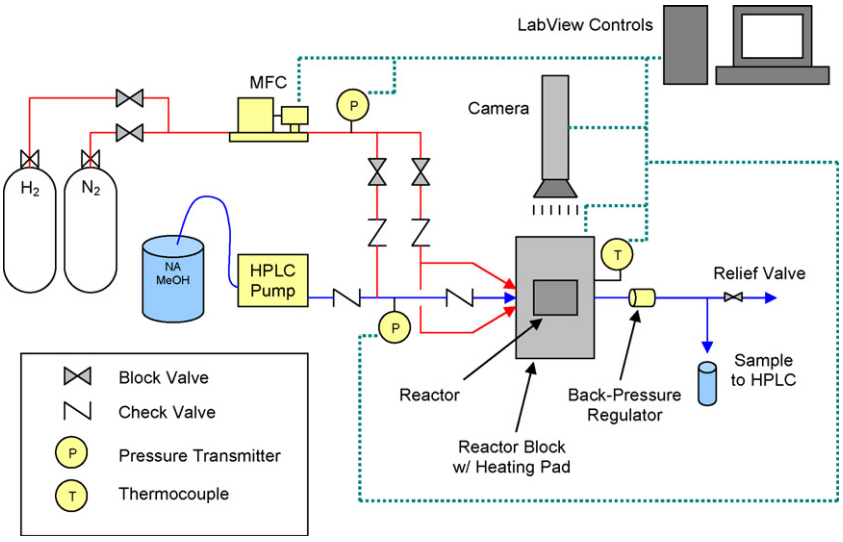

Fig. 6. Schematic of experimental setup.

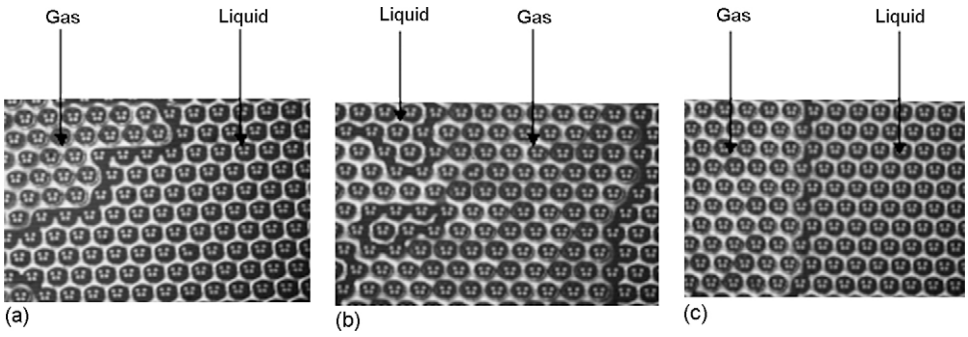

Fig. 7. (a) Liquid-dominated flow regime; (b) transitional flow regime; (c) gas-dominated flow regime.

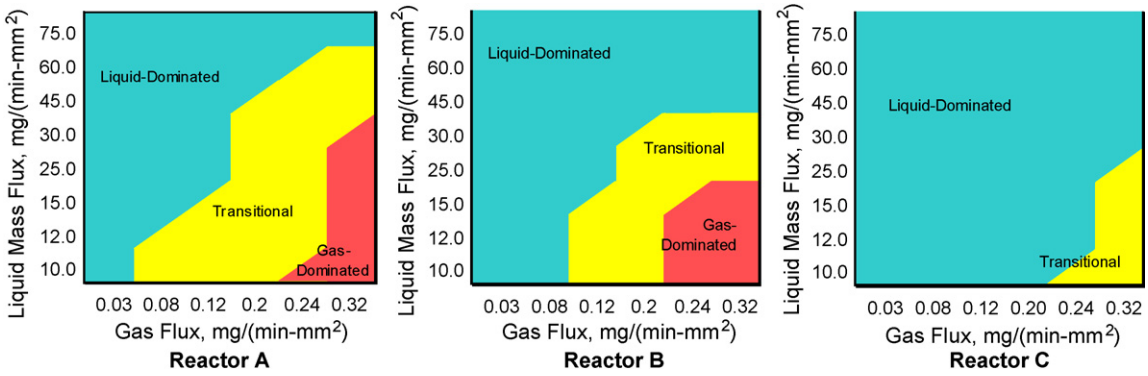

Fig. 8. Flow maps for Reactors A–C.

gas flow rates ranging from 2 to 20 sccm, in the absence of catalyst. We noted differences in behavior with changing conditions and approximated borders between the three flow regimes (Figs. 7–9).

With the flow maps established, we used the primary design, Reactor A, for kinetic experiments. We measured reaction conversion and selectivity at each point on the map. Reactor conditions were 30 °C and 25 psia for all kinetic experiments. The feed solution was approximately 16% nitroanisole by weight. Catalyst was manually loaded by inverting the reactor and applying vacuum to draw the catalyst through the inlet port. Tapping the reactor against the countertop caused the catalyst to move down the channel and settle amongst the traps. Our loading technique permitted coverage of 70–80% of the traps in the reactor, representing approximately 6 mg of catalyst for each run. For each set of conditions, we sampled the reactor outlet periodically over the course of approximately 1 h. Samples were analyzed offline in an HPLC to measure the weight fractions of *o*-nitroanisole and *o*-anisidine, from which we calculated the conversion and selectivity. After each run, we regenerated catalyst and evaporated any residual liquid by heating to 300 °C for 10 min.

4. Results and discussion

Because this particular microchannel is rectangular-shaped with a high width-to-depth ratio, it cannot be considered a capillary or cylindrical channel. Thus, the conventional nomenclature of bubble, slug, and trickle flow is not applicable to our geometry. Instead, "gas-dominated," "liquid-dominated," and "transitional" are more appropriate terms. Fig. 7 illustrates these flow regimes with overhead pictures of the reactor.

Liquid- and gas-dominated flows are characterized by stable patterns in which the continuous phase impedes movement of the non-continuous phase throughout the channel. For example, in liquid-dominated flow, 80% or more of the channel volume is occupied by liquid, with several small pockets of gas. In gas-dominated flow, large gas pockets persist and force liquid to channel around them. The gas–liquid interfaces in these flow regimes are largely stagnant.

Transitional flow is characterized by an unstable pattern in which gas and liquid compete for space within the channel. This competition causes a periodic (30–90 s) refreshing of the gas–liquid pattern, so that in addition to significant interfacial area, high turbulence is exhibited within the channel. Pockets of gas, upon refreshing, often leave behind traps surrounded by a droplet of liquid. The small distance (~15 μm) between posts likely prevents gas from overcoming the liquid surface tension, and leaves behind "wetted" traps within the gas pocket, a desirable effect we will discuss further when we present the reaction results. The presence of wetted traps is another indicator of transitional flow. It is important to note that the modified terminology is intended only to help visualize the correct flow behavior, and that liquid-dominated/transitional/gas-dominated are analogous to bubble/slug/trickle in the context of the mass transfer arguments presented in Section 1.

Although there are no quantitative measures to determine the particular gas–liquid flow regime at hand, we identify the bor-

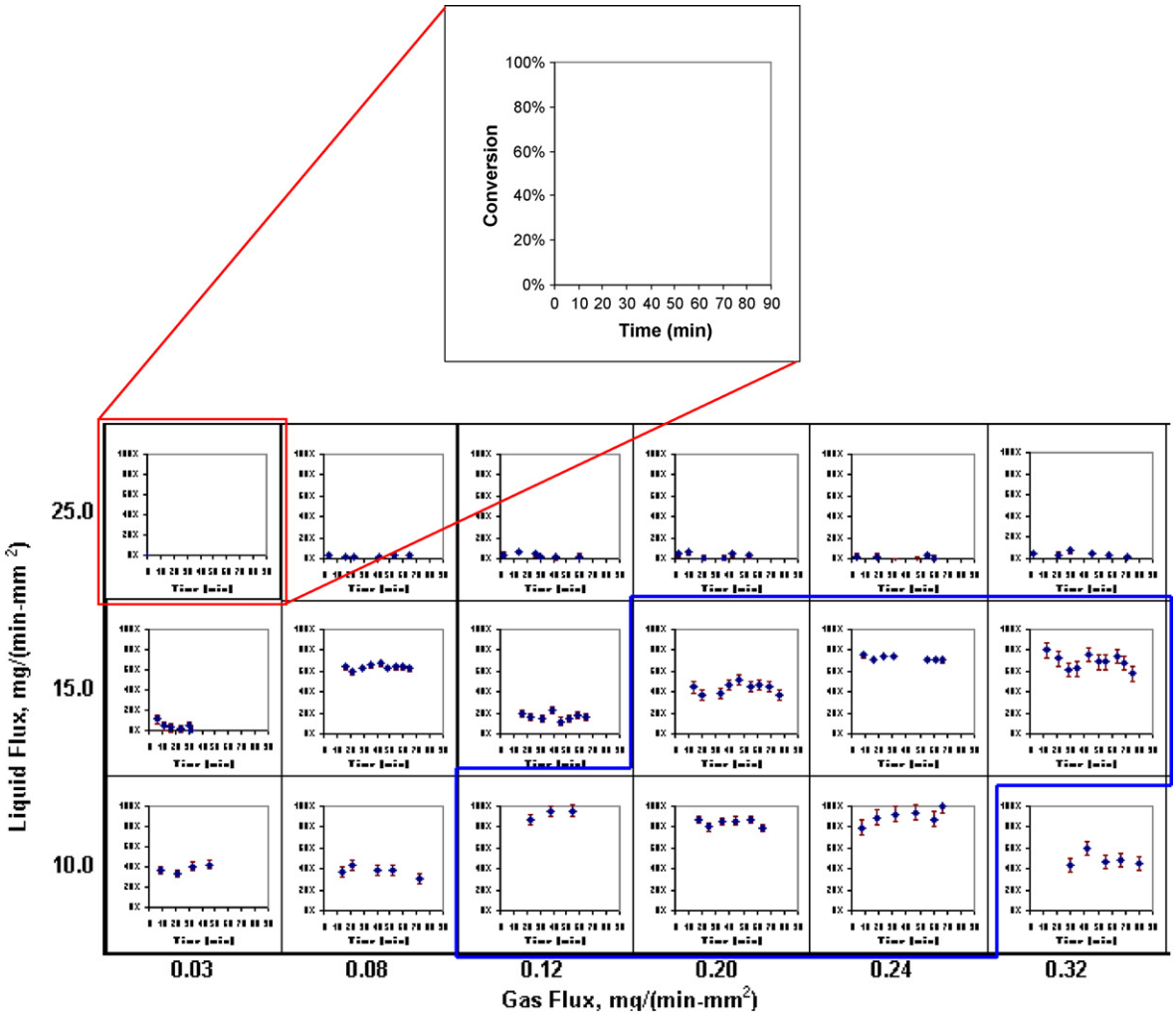

Fig. 9. Conversion results (30 °C, 25 psia).

ders between the flow regimes based on two key and somewhat reliable indicators: the refreshment frequency of the gas–liquid pattern and the presence of wetted traps. Based on our observations, the flow map for each reactor is shown below.

The flow maps are best understood from the perspective of relative resistance to gas and liquid flow throughout the channel. If one resistance is far less than another, then that particular phase will dominate; if the resistances are similar, competition between the phases exists, and the transitional regime prevails. The largest region of transitional flow is in Reactor A. We theorize that the smaller trap spacing (75 μm) provides greater resistance to liquid flow throughout the channel so that gas flow is more easily able to compete, resulting in larger areas of transitional and even gas-dominated flow. Conversely, the large spacing (150 μm) of Reactor B causes a portion of the transitional region to give way to liquid-dominated flow. Pressure drop across the bed lends support to this assertion. The pressure drop, estimated from the two-phase Ergun equation [33], is approximately five times greater in Reactor A than Reactor B (0.24 psi versus 0.045 psi for a representative set of conditions). The narrow liquid channel of Reactor C serves to increase liquid velocity and further enhance its advantage over gas. When coupled with 150 μm trap spacing, the liquid-dominated region of Reactor C is the largest of any of the three reactors. It is only at its very highest flow rates that the gas could overcome resistance from the liquid and cause transitional flow within the channel.

We obtain conversion results from Reactor A for the lower portion of the flow map. In Fig. 9, each chart shows the conversion plotted against time. Error bars represent one standard deviation for each particular set of samples. We observe no significant catalyst deactivation across the 1 h time span of each run.

The highest conversion in Fig. 9 occurs in the highlighted area. This range coincides with the transitional flow regime in Fig. 8. Conditions outside the transitional region experience significantly lower conversion. We also note that within a given flow regime, conversion is higher with increasing liquid flux, indicating the influence of liquid residence time. For all runs, the selectivity towards *o*-anisidine is nearly 100%, indicating that no side reactions occur.

The conversion results are consistent with our premise that the best reactor performance would fall within the flow regime exhibiting either the best gas–liquid or liquid–solid mass transfer characteristics. In our case, this is transitional flow, with its con-

Table 2
Gas–liquid interfacial area

	Area per catalyst trap (mm^2)	Number of traps	Total interfacial area (mm^2)	Volume of liquid channel (mm^3)	Total contact area (m^2/m^3)
Reactor A	0.0942	14,082	1320	108	6140
Reactor B	0.0942	6,426	606	108	2800
Reactor C	0.0942	3,806	359	108	1660

tinually refreshing pattern and high gas–liquid interfacial area. From our analysis of the flow maps, Reactor A, with the largest region of transitional flow, would be best suited for this type of reaction.

Though their mass transfer characteristics are similar, there is one outstanding difference between conventional slug flow and our observed transitional flow. In slug flow within a capillary, the refreshing occurs by recirculation around the boundary of each slug. In general, slugs do not disturb the structure of adjacent slugs, and the pattern of alternating gas and liquid from one end of the channel to the other is maintained. In the analogous regime in the catalyst-trap reactor, the refreshing in transitional flow affects the entire channel, as though the pattern is wiped clean and then redrawn in a different, usually random, way. Thus, it could be argued that the turbulence brought on by transitional flow enhances not only gas–liquid, but also liquid–solid mass transfer, making it clearly the preferred regime for the reaction.

Our plug-flow model, used initially for design of the reactor, significantly under-predicts the measured conversion across our range of experimental conditions. The model makes the assumption that the reaction is controlled by gas–liquid mass transfer, but even after adjusting the interfacial area parameter in Eq. (2), a_h, to large values, the experimental conversion remains much higher. Refinements to the model, made after further experiments, are to be discussed in a future paper.

A possible explanation for deficiencies in the model is the presence of wetted versus non-wetted catalyst traps. As we discussed above, when the gas pattern refreshes it often leaves behind traps encased in droplets of liquid. An array of several thousand traps covered by liquid droplets approximately 100 μm in diameter creates extraordinary surface area. Such a cylinder itself has a surface-to-volume ratio of 40,000 m^2/m^3. If coupled with the proper refreshing gas–liquid pattern the traps would function as a network of miniature batch reactors, where refreshing periodically sweeps away the products and introduces new reactants. The droplets' small size would give very short diffusion distances for hydrogen, allowing for excellent transport of dissolved hydrogen throughout the liquid phase, and high reaction conversion. Fig. 10 shows a snapshot of the reactor in operation with areas of wetted and non-wetted traps.

We can use our example of the 100 μm cylinder representing a wetted trap to estimate the gas–liquid interfacial area in the channel. A reasonable estimate is that half the traps are wetted during periods of transitional flow, so we can calculate the ratio of interfacial area to channel volume, similar to the a_h parameter. These values are shown in Table 2 as the "Total Contact Area". While typical values of a_h are on the order of 1000 m^2/m^3 for macroscale equipment such as packed absorbers and strippers,

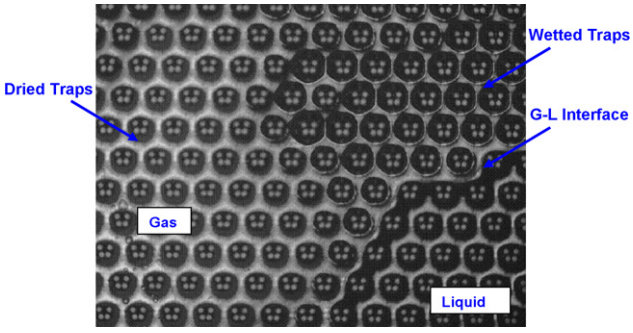

Fig. 10. Reactor photograph of dried vs. wetted traps.

we can see that the values are much higher for the microreactors, particularly Reactor A.

By altering the reactor design, it is possible to enhance both the extent of the transitional flow region and the gas–liquid interfacial area created within the reactor, thereby optimizing subsequent reaction performance.

5. Conclusions and future work

Using three variations of our reactor design, we define regimes of liquid-dominated, gas-dominated, and transitional flow based on certain key characteristics of the gas–liquid behavior. As the trap density decreases, resistance to liquid flow decreases, and the desirable region of transitional flow, or competition between gas and liquid, grows smaller. Decreasing liquid channel width increases the resistance to gas flow, thus extending the region of liquid-dominated flow.

We measure conversion and selectivity at each point on the flow map for our primary design, Reactor A. We find that the highest conversion falls within the transitional flow regime, as the reaction is mass-transfer-controlled, rather than kinetically controlled. The turbulence induced by transitional flow provides the best gas–liquid and liquid–solid mass transfer. Experimental conversion is significantly higher than predicted by our first-pass design model. We attribute the enhancement to the presence of wetted traps functioning as a network of small batch reactors and providing a large gas–liquid interfacial area. Wetted traps are prominent in the transitional flow regime, so a reactor design that maximizes the region of transitional flow is well-suited for this type of reaction.

For future work, the conversion results should be duplicated at a higher hydrogen partial pressure. Based on non-reactive experiments at pressures of 160 psia, we observe that reactor pressure has no effect on the flow map for a given design, but we expect a benefit to conversion from the increase in hydro-

gen liquid-phase solubility. Finally, we can explore the effect of wetted traps by revising our plug-flow model to include some prediction of interfacial area and residence time in a series of tiny batch reactors.

References

[1] W. Ehrfeld, V. Hessel, H. Lowe, Microreactors: New Technology For Modern Chemistry, Wiley, 2000.
[2] K.F. Jensen, Chem. Eng. Sci. 56 (2001) 293–303.
[3] K.F. Jensen, Nature 393 (1998) 735.
[4] M.H. AlDahhan, F. Larachi, M.P. Dudukovic, A. Laurent, Ind. Eng. Chem. Res. 36 (1997) 3292–3314.
[5] A. Gavriilidis, P. Angeli, E. Cao, K.K. Yeong, Y.S.S. Wan, Trans. IChemE 80 (2002) 3.
[6] O. Worz, K.P. Jackel, Th. Richter, A. Wolf, Chem. Eng. Sci. 56 (2001) 1029–1033.
[7] P.L. Mills, R.V. Chaudhari, Catal. Today 37 (1997) 367.
[8] E.H. Stitt, Chem. Eng. J. 4025 (2002) 1–14.
[9] S. Tadepalli, R. Halder, A. Lawal, Chem. Eng. Sci. 62 (2007) 2663–2678.
[10] H. Surangalikar, X. Ouyang, R.S. Besser, Chem. Eng. J. 93 (2003) 217.
[11] H.S. Fogler, Elements of Chemical Reaction Engineering, fourth ed., Prentice Hall, PTR, 2006.
[12] M. Kreutzer, F. Kapteijn, J. Moulijn, J. Heiszwolf, Chem. Eng. Sci. 60 (2005) 5895–5916.
[13] J.L. Xu, P. Cheng, T.S. Zhao, Int. J. Multiphase Flow 25 (1999) 411.
[14] K.A. Triplett, S.M. Ghiaasiaan, S.I. Abdel-Khalik, D.L. Sadowski, Int. J. Multiphase Flow 23 (1999) 377.
[15] M.K. Akbar, D.A. Plummer, S.M. Ghiaasiaan, Int. J. Multiphase Flow 29 (2003) 855.
[16] W.L. Chen, M.C. Twu, C. Pan, Int. J. Multiphase Flow 28 (2002) 1235.
[17] F. Kapteijn, T.A. Nijhuis, J.J. Heiszwolf, J.A. Moulijn, Catal. Today 66 (2001) 133.
[18] J. Heiszwolf, M. Kreutzer, M. van den Eijnden, F. Kapteijn, J. Moulijn, Catal. Today 69 (2001) 51–55.
[19] P.H. Brahme, H.G. Vadgaonkar, P.S. Ozarde, M.G. Parande, J. Chem. Eng. Data 27 (1982) 461–462.
[20] J.D. Seader, E.J. Henley, Separation Process Principles, first ed., Wiley, 1998.
[21] R.V. Chaudhari, M.G. Parande, P.A. Ramachandran, P.H. Brahme, IChemE Symposium Series No. 87.